Article:
Campbell, R., Konar, S., Hunter, S. et al. (2 more authors) (2018) Labile low-valent tin azides: syntheses, structural characterization, and thermal properties. Inorganic Chemistry, 57 (1). pp. 400-411. ISSN 0020-1669

https://doi.org/10.1021/acs.inorgchem.7b02621

Labile Low-Valent Tin Azides: Syntheses, Structural Characterisation, And Thermal Properties

Rory Campbell,[a] Sumit Konar,[b] Steven Hunter,[b] Colin Pulham,[b] Peter Portius*[a]

[a]*Department of Chemistry, University of Sheffield, Brook Hill, S3 7HF, U.K.*

Email: p.portius@sheffield.ac.uk

[b]*EaStChem School of Chemistry, University of Edinburgh, David Brewster Rd., EH9 3FJ, U.K.*

Abstract. The first two examples of the class of tetracoordinate low-valent, mixed-ligand tin azido complexes, $Sn(N_3)_2(L)_2$, are shown to form upon reaction of $SnCl_2$ with NaN_3 and SnF_2 with Me_3SiN_3 in either pyridine or 4-picoline (**2**, L = py; **3**, L = pic). These adducts of $Sn(N_3)_2$ are shock- and friction insensitive and stable at r.t. under an atmosphere of pyridine or picoline, respectively. A new, fast and efficient methods for the preparation of $Sn(N_3)_2$ (**1**) directly from SnF_2, and by the step-wise de-coordination of py from **2** at r.t., is reported that yields **1** in microcrystalline form, permitting powder diffraction studies. Reaction of **1** with a non-bulky cationic H-bond donor forms the salt-like compound $\{C(NH_2)_3\}Sn(N_3)_3$ (**4**) which is comparably stable despite its high nitrogen content (55%) and the absence of bulky weakly coordinating cations that are conventionally deemed essential in related systems of homoleptic azido metallates. The spectroscopic and crystallographic characterisation of the polyazides **1**-**4** provides insight into azide-based H-bonded networks and unravels the previously unknown structure of **1** as an important lighter binary azide homologue of $Pb(N_3)_2$. The atomic coordinates for **1** and **2**-**4** were derived from powder and single crystal XRD data, respectively; those for **1** are consistent with predictions made by DFT-D calculations under periodic boundary conditions.

Introduction

Binary azides, $E(N_3)_n$, exist of all *s*-block, most *p*-block and a number of *d*-block elements, many of which have well-established synthetic procedures.[1-4] Exceptions to this notion exist in particular among the binary azides of lighter, more electronegative elements, such as those in Group 14 (E = Si - Sn, n = 2 or 4). These nitrogen-rich azides are predicted to possess primarily covalent E-N bonds between azido groups and the coordination centres, as a result of which the gap between ground state and the transition state toward dinitrogen elimination is comparably small and the compound stability low. The combination of high endothermicity and sensitivity toward external stimuli renders the characterisation of such azides challenging. Accordingly, only few solid state structures of these simple azides are unknown. In the *p*-block, these include $Pb(N_3)_2$ (and polymorphs),[5, 6] TlN_3,[7] $As(N_3)_3$ and $Sb(N_3)_3$.[8-10] However, the kinetic stability of inorganic azides can be increased dramatically by the coordination of ancillary ligands.[11-14] The binary Lewis-acidic azides $Si(N_3)_4$, $Ge(N_3)_4$, $Ge(N_3)_2$ and $Sn(N_3)_4$, for instance, have been shown to form well-defined charge-neutral adducts with Lewis bases, of the types $(N_3)_4E(L_2)$ (E = Si, Ge, Sn, L_2 = bpy, phen) [15-17] and $E(N_3)_2L$ (E = Ge, L = N-heterocyclic carbene), respectively.[18] The class of Sn(II) azides, in particular, includes monoazides $Sn(N_3)$(ATI),[19] and a 1 : 1 adduct with $Ag(Tp^{CF3})$,[20] $SnN_3(mes_2DAP)$,[21] $SnN_3\{HC(MeC{=}NAr)_2\}$, Ar = Ph[22] or 2,6-^{i}Pr-C_6H_3,[23] $SnN_3\{HC(PPh_2{=}NSiMe_3)_2\}$[24] and triazido stannate, $Sn(N_3)_3^-$ [25] (see Table 1 and abbreviations in the caption). Coordinatively unsaturated and sterically less protected Sn(II) azido complexes on the other hand tend to dimerise ($Sn(N_3)N{=}IPr$,[26] $Sn(N_3)(OCH_2CH_2NMe_2$ [27]). No diazide tin(II) complexes have been reported. The first synthetic method for the preparation of tin diazide (**1**)[28] was described only recently in a report on binary metal azides that involves the oxidation of Sn metal by AgN_3 in water-free liquid ammonia at low-temperature. However, the structure of **1** remained undetermined. Compound **1** was reported to be sensitive and explosive and resembles in these properties its homologue, lead(II) azide,[29] a well-established initiatory explosive that is known for its low water solubility and comparably high stability toward hydrolysis and heat.[30] The relationship between stability and molecular and crystal structure of azides is determined not only by the nature of the coordination centres and counter ions but also by their interaction. In systems with similarly high reactive nitrogen content, it is usually those compounds in which the N_3 groups are involved in the least covalent interactions that possess the greater activation barrier to N_2 elimination. The influence of intermolecular interaction and vibrational energy distribution on stability is less well understood; this includes hydrogen bonding. Recently, it was shown that in a salt-like compound containing triazidostannate, $Sn(N_3)_3^-$, relatively large, weakly coordinating PPh_4^+ cations[25] produce an effect similar to that induced by bulky ligands, in keeping the nitrogen content low (21.6 %) and separating the N_3 anions, thus retarding shockwave propagation and reducing sensitivity (for other PPh_4-containing homoleptic polyazidometallate, see ref.s [10, 31-35]). The combination of $Sn(N_3)_3^-$ with

suitable nitrogen-rich cations may confer a similar phlegmatising effect by virtue of hydrogen bonding *without* diluting nitrogen content.[4]

Here we describe the synthesis of the first two examples of the class of tetracoordinate $Sn(N_3)_2(L)_2$ complexes and their utility for the preparation of a hydrogen-bonded guanidinium triazidostannate, $\{C(NH_2)_3\}Sn(N_3)_3$, and of tin diazide, $Sn(N_3)_2$. We report a new, fast and efficient method for the preparation of $Sn(N_3)_2$ from SnF_2 and $Me_3Si\text{-}N_3$, which yields the binary azide in microcrystalline form, permitting powder diffraction studies. The spectroscopic and crystallographic characterisation of the diazides provides insight into azide-based H-bonded networks and unravels the previously unknown structure of $Sn(N_3)_2$ as an important lighter binary azide homologue of $Pb(N_3)_2$. PXRD and single-crystal XRD studies were complemented by DFT-D calculations. Pyridine and 4-picoline coordinate reversibly to $Sn(N_3)_2$ under formation of the shock insensitive adducts which are stable at r.t. only under an atmosphere of pyridine or picoline, respectively. Furthermore, $Sn(N_3)_2$ reacts with guanidinium azide to form a salt-like compound with high nitrogen content and lower sensitivity.

Results and Discussion

Syntheses

p-Block azides have often been synthesised by fluorine / azide exchange reactions using azido(trimethyl)silane as the azide group transfer reagent.[36-38] This method benefits from mild reaction conditions arising from the strong enthalpic preference for Si–F over Sn–F bonds, and from the facile removal of the gaseous TMS-F by-product. The preparation of the tetravalent tin complex $Sn(N_3)_4(py)_2$ from SnF_4 (py = pyridine, pic = 4-picoline)[17] demonstrates the effectiveness of this method. Under similar conditions, SnF_2 reacts with $TMS\text{-}N_3$ in pyridine or 4-picoline solutions. In-*situ* FTIR spectra of these reaction mixtures show that within two hours the absorptions due to the asymmetric N_3 stretch of $TMS\text{–}N_3$ at 2138 cm^{-1} are replaced by two new bands at 2077 cm^{-1} and 2057 cm^{-1} (in pyridine; 2076 and 2057 cm^{-1} in picoline), indicating the formation of a new covalent azide species. The analogous reactions[17] involving SnF_4 are much slower which we ascribed primarily to the lower solubility of SnF_4 in these solvents. Crystals obtained from the reaction solutions were used for structural, spectroscopic and thermochemical studies (*vide infra*), which revealed the formation of the low-valent tetracoordinate polyazido complexes $Sn(N_3)_2(py)_2$ (**2**) and $Sn(N_3)_2(pic)$ (**3**) (Scheme 1). Both complexes also form by reaction of $SnCl_2$ with NaN_3. This method, however, requires great excess of the ionic azide transfer reagent and the removal of NaCl from intermediate stages in the N_3 / Cl exchange. In reaction solutions obtained from this method, the mono(azido) species $SnCl(N_3)(py)_2$ (ν_{as} = 2069 cm^{-1}) could be observed. Intriguingly, crystalline **2** is sparingly soluble in MeCN, THF and Et_2O and CH_2Cl_2, and decomposes, under these solvents, into another microcrystalline solid (compound **1**) from which all IR absorption bands of coordinated pyridine and solvent are absent. The same material (**1**) is eventually formed if **2** is exposed to a dynamic vacuum at

r.t. The analogous 4-picoline complex **3**, however, is stable under these conditions. Observations of the responses toward electrostatic discharge and friction show that **1** can be handled only with great care and its sensitivity exceeds that of $Pb(N_3)_2$.[39] It is also air sensitive and discolours under an Ar atmosphere if exposed to sunlight. PXRD measurements allowed for a structure determination (*vide infra*) which revealed that it consists solely of tin(II) azide which had been synthesised previously by Schnick *et al.* for the first time.[28] Compound **1** reacts readily with Lewis bases such as guanidinium azide, $(G)N_3$, to form guanidinium triazidostannate (**4**), $(G)Sn(N_3)_3$. Compound **4** also forms directly in mixtures of SnF_2, TMS–N_3 and $(G)N_3$. Notably, the compound shows no sensitivity toward friction and impact despite containing a binary azide species and an overall nitrogen content of 55% *w*/*w*.

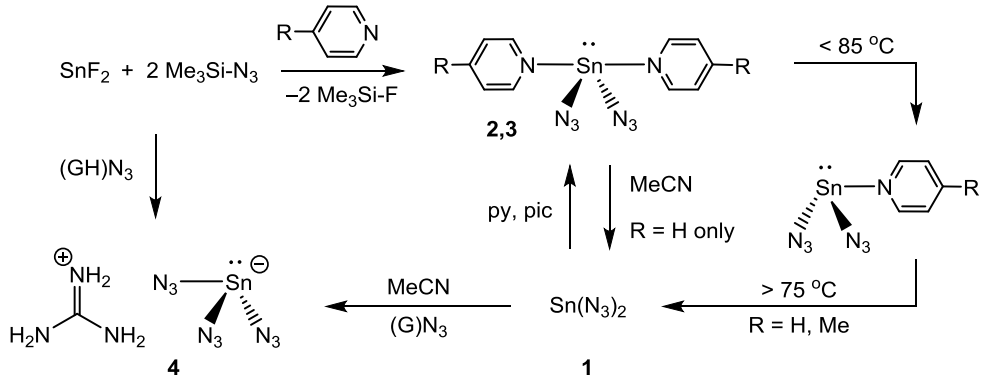

Scheme 1. Synthesis and reactivity of the tin(II) polyazides **1-4** , R = H (**2**), Me (**3**), G = $C(NH_2)_3$, py = pyridine, pic = 4-methylpyridine.

Compound **4** is soluble in CH_3CN and THF, but completely insoluble in CH_2Cl_2, whereas **1**, **2** and **3** are sparingly soluble in these solvents and soluble in 4-picoline and pyridine. All tin(II) azides (**1** – **4**) are air sensitive, particularly so in solution. I*n-situ* IR spectra showed that the exposure of a solution of **4** to air over the course of an hour resulted in almost complete hydrolysis to hydrazoic acid (HN_3) and oxidation to $(G)_2Sn(N_3)_6$.

Crystal structures of compounds 1-4

Molecular structures of the solid azides were determined by X-ray single crystal diffraction (**2**-**4**) and powder diffraction methods (**1**) (see experimental section and pages S5-S11 for crystallographic details).

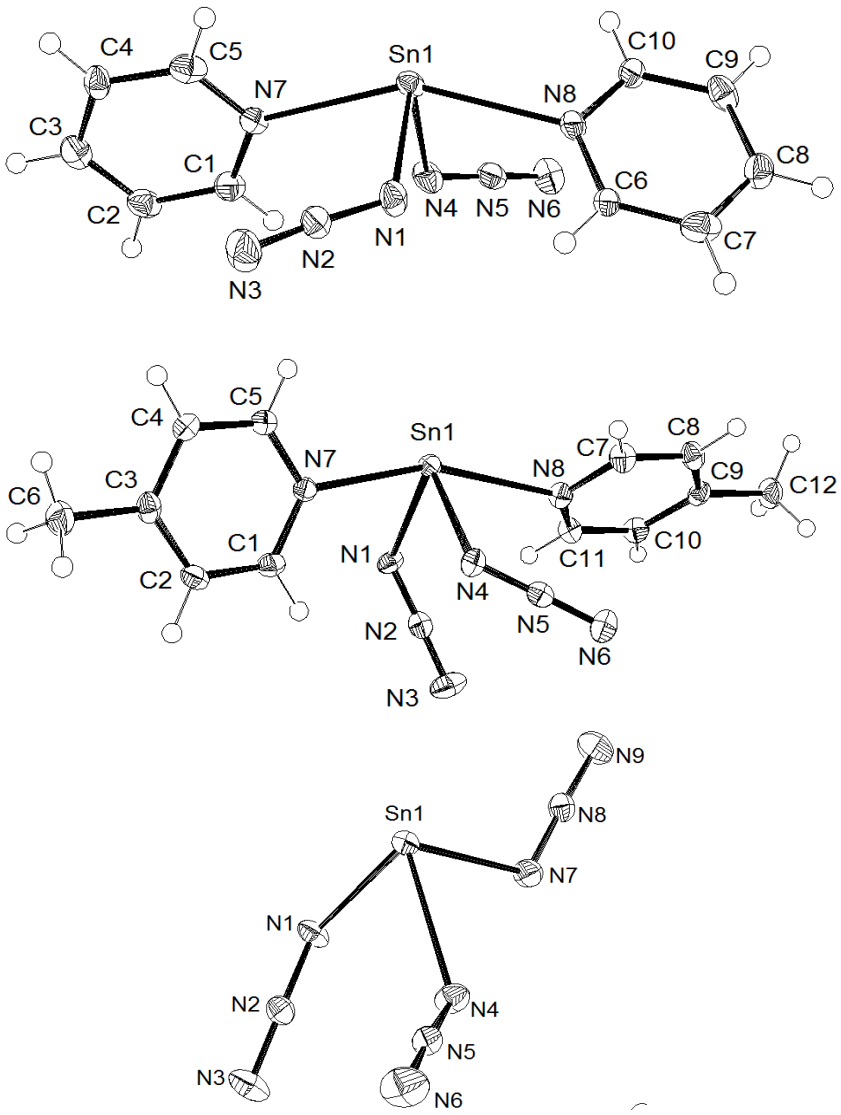

Figure 1. Thermal ellipsoid drawing of the asymmetric unit in the crystal structure of $Sn(N_3)_2(py)_2$ (**2**, top) and $Sn(N_3)_2(pic)_2$ (**3**, middle) and $(G)Sn(N_3)_3$ (**4**, bottom, cation not shown) at 100 K; thermal ellipsoids at the 50% probability level. Selected bond lengths [Å] and angles [°] **2**: Sn1–N1 2.178(5), Sn1–N4 2.195(6), Sn1–N7 2.468(5), Sn1–N8 2.472(5), N1–N2 1.216(8), N2–N3 1.139(8), N4–N5 1.209(8), N5–N6 1.143(9); N1–Sn1–N4 92.0(2), N7–Sn1–N8 153.14(16). Torsion angle between calculated (LS) mean planes of pyridine rings is 71.75°; **3**: Sn1–N1 2.1992(17), N1–N2 1.213(2), N2–N3 1.145(2), Sn1–N4 2.2396(17), N4–N5 1.210(2), N5–N6 1.154(2), Sn1–N7 2.4203(16), Sn1–N8 2.5858(17); Sn1–N1–N2 119.45(13), N1–N2–N3 178.1(2), Sn1–N4–N5 122.36(13), N4–N5–N6 176.7(2), N1–Sn1–N4 86.53(6), N7–Sn1–N8 158.90(5); **4**: Sn1–N1 2.2380(19), N1–N2 1.206(3), N2–N3 1.143(3), Sn1–N4 2.2736(19), N4–N5 1.198(3), N5–N6 1.156(3), Sn1–N7 2.2142(19), N7–N8 1.208(3), N8–N9 1.150(3); Sn1–N1–N2 118.28(15), N1–N2–N3 179.1(3), Sn1–N4–N5 126.61(16), N4–N5–N6 177.5, Sn1–N7–N8 118.27(15), N7–N8–N9 178.0(2), N1–Sn1–N4 83.00(7), N4–Sn1–N7 81.98(7), N1–Sn1–N7 88.77(7).

The crystals of compound **2** and **3** consist of tin complexes (Fig. 1, top and middle) with disphenoidal coordination skeletons in which two azido (N_3) ligands occupy *cis*-equatorial sites and two pyridine (py) or 4-picoline (pic) ligands the *axial* coordination sites. Compound **4** (Fig. 1, bottom), on the other hand, adopts a salt-like structure containing trigonal pyramidal triazidostannate(1−) complexes and guanidinium counter ions. The shapes of the coordination skeletons of the tin-containing complexes in **2**, **3** and **4** are affected by the presence of lone electron pairs (*i*), N_3 ligand bridging (*ii*) and

intermolecular hydrogen bonding (*iii*) (*vide infra*) and conform therefore only approximately with the geometries of the $AB_2B'_2E$ (**2**, B' = py; **3**, B' = pic) and AB_3E (**4**) models required by VSEPR

The most characteristic feature of the new structures, however, is the difference in the coordinative bond lengths between high- and low-valent analogues. In comparison with high-valent $Sn(N_3)_4L_2$, L = py (**2a**), pic (**3a**) and $Sn(N_3)_6^{2-}$ (**4a**),[17, 40] the low-valent complexes **2**-**4** feature Sn–N_α bonds to the N_3 ligands that are *ca*. 0.1 Å longer while the Sn^{II}-N_L bonds to py and pic ligands are elongated even further (*ca*. 0.2 Å). The pyridine-type ligands are equidistant from the coordination centre in the complexes **2** (2.47 Å), **2a** and **3a**, but not in **3** (2.59 Å vs. 2.42 Å); see discussion below). The bond elongation can be ascribed to the shielding of nuclear charge by a lone electron pair at the coordination centre that is absent in high-valent complexes. The angle included between the coordination centre and the axial pyridine-type N ligators, N_L-Sn(II)-N_L, which was found to be 154° (**2**) and 159° (**3**), respectively, indicates that these ligands are repelled from the domain of a stereochemically active lone pair. The angle shared by the equatorial N_3 ligands, on the other hand, is close to 90° and ranges between 82° and 92° in the structures **2** to **4**, like the recently reported structure of $Sn(N_3)_3^-$ in $(PPh_4)Sn(N_3)_3$.[25] Complexes with low-valent main group centres (Table 1) often have a lone pair that affects their reactivity and coordination geometry. The unsupported Ag–Sn bond of the adduct $HB\{3,5\text{-}(CF_3)_2pz\}_3Ag\text{-}Sn(N_3)(^nPr_2ATI)$ (*vide supra*), for instance, involves the lone pair on Sn rather than azido ligands bridging Ag with Sn centres.[41] A comparison with SF_4, for instance, reveals that the influence of the lone pair on the *trans* ligands (B') in **2** and **3** is substantial. In SF_4, the related angle (173°) deviates far less from linearity required by perfect disphenoidal geometry of the $AB_2B'_2E$ model. Intriguingly, the lengths difference between N_α–N_β and N_β–N_γ bonds (ΔNN) correlates inversely with the Sn–N bond lengths and is approximately 1 pm greater in **2**, **3** in comparison to **2a**, **3a** (Fig. 2). This finding suggests that Sn–N_α bonds of the low-valent Sn(II) complexes are less covalent than those of the Sn(IV) azides.

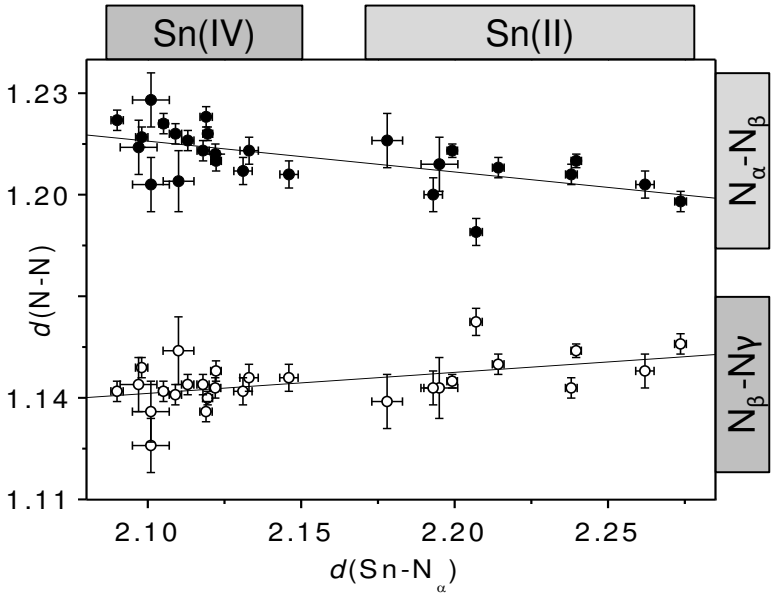

Figure 2. Correlation of crystallographically determined Sn-N_α bond lengths with those of N_α-N_β (●) and N_β-N_γ (○) in the polyazides of Sn(II) (**2**-**4**, $(PPh_4)Sn(N_3)_3$), and Sn(IV) (**2a**-**4a**, $Sn(N_3)_4(bpy)$, $Sn(N_3)_4(phen)$); the error bars show the estimated standard deviations (1σ).

The unsaturated coordination sphere surrounding low-valent tin usually allows for weak secondary interactions between adjacent molecules in a dimeric or polymeric fashion. Halide or pseudohalide ligands, such as those in the bromo analogue of **2**, allow formation of infinite three-dimensional coordination network structures in the solid state (alternating short / long Sn-Br contacts in $SnBr_2(py)_2$).[42] The coordinative Sn–N_L bonds to the pyridine ligands in **2** are slightly shorter at 2.468(5) Å and 2.472(5) Å than those found in $SnBr_2(py)_2$ at 2.557(4) Å. In the crystals of **3** and **4**, but not **2**, dimeric structures (Fig. 3) are present featuring an asymmetric $\mu_{1,1}$ bridging coordination of two N_3 ligands linking two Sn centres in the nearly planar fashion already encountered previously in $(PPh_4)Sn(N_3)_3$,[25] with short Sn–N_α (2.21-2.27 Å) and long Sn···N_α (2.65-2.83 Å) distances and N_α–Sn···N_α angles close to 120°. The Sn–N_α bond involving the bridging azide group in **3** is slightly shorter (2.1992(17) Å) than the other (2.2396(17) Å) due to the absence of the *trans*-influence. This *trans*-influence can also be observed in crystals of compounds **4** and $(PPh_4)Sn(N_3)_3$, where the longest Sn–N_α bond is found opposite the shortest Sn···N_α interanionic contact. Even though the Sn···N_α bonds are considerably shorter than the sum of van der Waals radii of the atoms involved (3.72 Å),[43, 44] the fact that structure **2** does not exhibit this structural feature indicates that the Sn···N_α–N_α interactions between the tetracoordinate $Sn(N_3)_2L_2$ complexes are weak and can be disrupted if a different packing arrangement results in a greater total van der Waals force in the crystal.

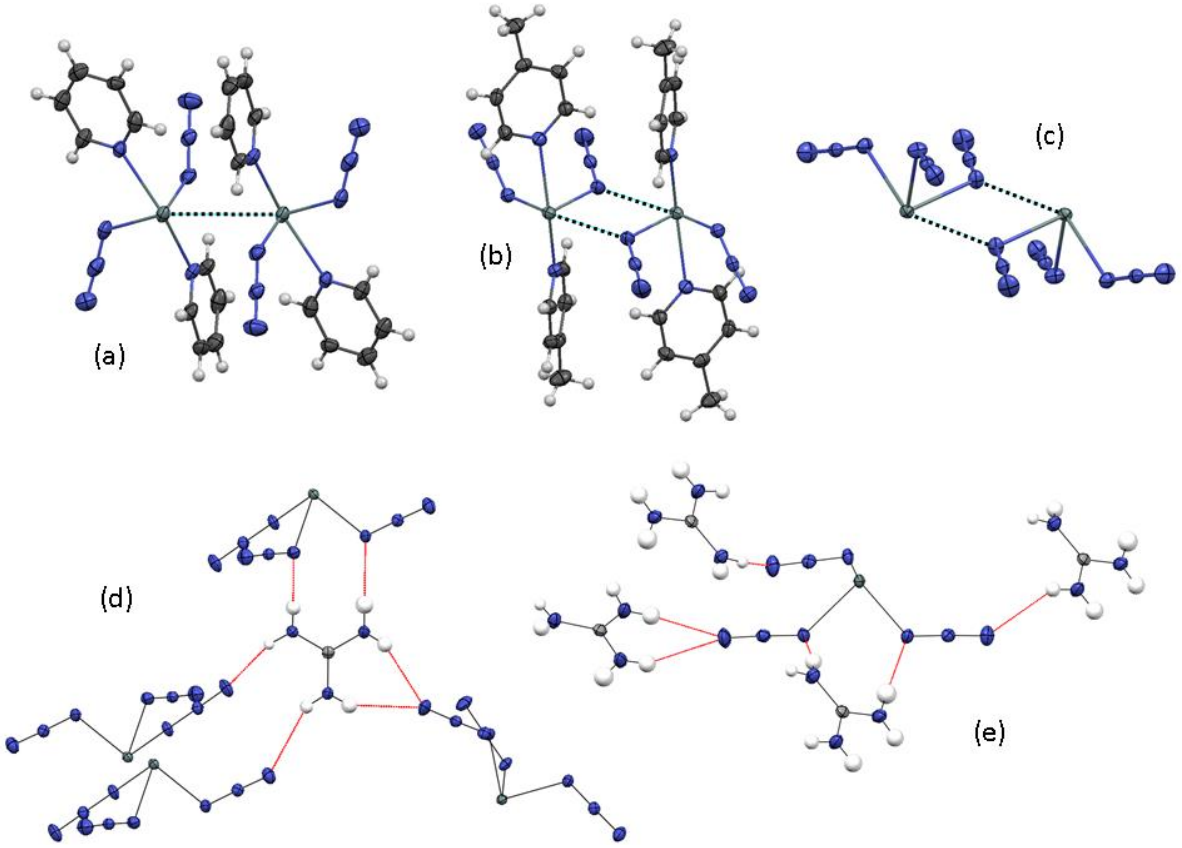

Figure 3. Shortest distances between azido complexes (dashed black lines) in the crystals of **2** (a), Sn-Sn = 3.75 Å, **3** (b), Sn-N = 2.83 Å and **4** (c), Sn-N = 2.65 Å); hydrogen bonds (red lines) arising from H-bond donor (d) and acceptor (e) in **4**; light grey H, dark grey C, blue N, turquoise Sn.

The crystals of **2** and **3** contain networks of *weak* C-H···N hydrogen bonds[45] (shortest *d*(D–A) / Å = 3.40 (**2**) and 3.47 (**3**) at D–H…A angles of 153° and 165°, respectively). The crystals of **4**, on the other hand, are dominated by *strong* N–H···N hydrogen bonds[45] (Fig. 3 (d) and (e)). Each of the guanidinium cations, which are stacked directly above one another along the crystallographic *c*-axis in alternating orientation, is bound by six normal hydrogen bonds (*d*(D–A) 2.96 to 3.32 Å, D–H…A 148° to 177°) to four $Sn(N_3)_3^-$ ions involving all hydrogen and most N_α and N_γ azide atoms (Fig. 3, bottom, Tables S1,S2). The H-bonding results in a three-dimensional network unlike the strongly H-bonded guanidinium salt $(G)BF_4$, which adopts a $G\cdots FBF_3$ sheet structure.[46] Intriguingly, the hydrogen bonding in **4** appears to induce high density. This notion is based on a comparison of the crystal structures of $G^+ Y^-$ and $PPh_4^+ Y^-$, $Y^- = N_3^-$,[33] $Sn(N_3)_3^-$,[25] which shows that in **4** the apparent spatial requirement of $Sn(N_3)_3^-$ is about 5 $Å^3$ less than in the related $(PPh_4)Sn(N_3)_3$ salt. Similar results are obtained by using independently determined volumes of the cations (p. S16, table S6).

The PXRD pattern of **1** (Fig. 5) was indexed to a primitive monoclinic unit cell and an initial Le Bail refinement carried out. The reflections systematically absent support the space group $P2_1/a$. This space group was used in the *superflip* program implemented in the JANA2006 suite which located most of the atomic positions.[47] As a control, the structure of $Sn(N_3)_2$ was calculated using density

functional theory including dispersion corrections (DFT-D) based on the preliminary unit cell. This calculation confirmed that the initial structure obtained by Rietveld refinement of the powder diffraction data (using *TOPAS*, Fig. 5) is likely to be correct. The structural results from DFT-D calculations were fed back into the refinement model to finalise the refinement of the experimental crystal structure. Based on single crystal diffraction data obtained for **2** and **3** (*vide supra*), chemically plausible sets of bond lengths and bond angle restraints were employed during this refinement, which include *a*) NNN angles for the N_3 group set to 180°; *b*) the bond lengths N_α-N_β and N_β-N_γ set to 1.20 Å and 1.15 Å, respectively, where N_α denotes the ligating nitrogen, and *c*) the total lengths of the N_3 group set to 2.35 Å. Theory and PXRD data are in very good agreement and both show the N_3 ligands forming $\mu_{1,1}$-bridges between tin centres in the direction of the *c*-axis. The computationally and experimentally determined crystal lattice parameters differ by no more than 5% and geometric parameters are in reasonable agreement as well (Table 2). A high degree of similarity is also indicated by the crystal packing similarity value of 0.9974 calculated with Mercury (part of CCDC's CSD system, RMS error of 5.2×10^{-5}).

Table 1. Shortest Sn-N distances in the crystal structures of **2**, **3**, and **4** compared to those of previously known tin(II) azides.

Compound [a]	d(Sn–N_α) / Å [b]	d(Sn···N_α) / Å	T / K	
(Tp^{CF3}Ag)Sn(N_3)(ATI)	2.157(4)	N/A	208	[c]
Sn(N_3)$_2$(py)$_2$ (**2**)	2.178(5), 2.195(6)	-	100	this paper
Sn(N_3)(mes$_2$DAP)	2.198(5)	2.909(5)	228	[d]
Sn(N_3)$_2$(pic)$_2$ (**3**)	2.1992(17), 2.2396(17)	2.8257(17)	100	this paper
(N_3–Sn–OCH$_2$CH$_2$NMe$_2$)$_2$	2.220(5)	N/A	158	[e]
(PPh$_4$)Sn(N_3)$_3$	2.196(4)-2.262(4)	2.673(4)	100	[f]
(G)Sn(N_3)$_3$ (**4**)	2.242(3)	2.653(3)	100	this paper
Sn(N_3)(ATI)	2.253(4)	2.873(4)	198	[c]
Sn(N_3)$_2$ (**1**)	2.38(2), 2.41(3)	2.51(3), 2.58(2)	r.t.	this paper

[a] ATI = *N*-(*n*-propyl)-2-(*n*-propylamino)troponiminate), Tp^{CF3} = hydrotris(3,5-bis(trifluoromethyl)pyrazolyl)borate, mes$_2$DAP = 2,4-dimethyl-*N*,*N*′-bis(2,4,6-trimethylphenyl)-1,5-diazapentadienyl, all other abbrevs. see introduction; [b] range of independent distances, [c] ref. [20]; [d] ref. [21], [e] ref. [27], [f] ref. [25]

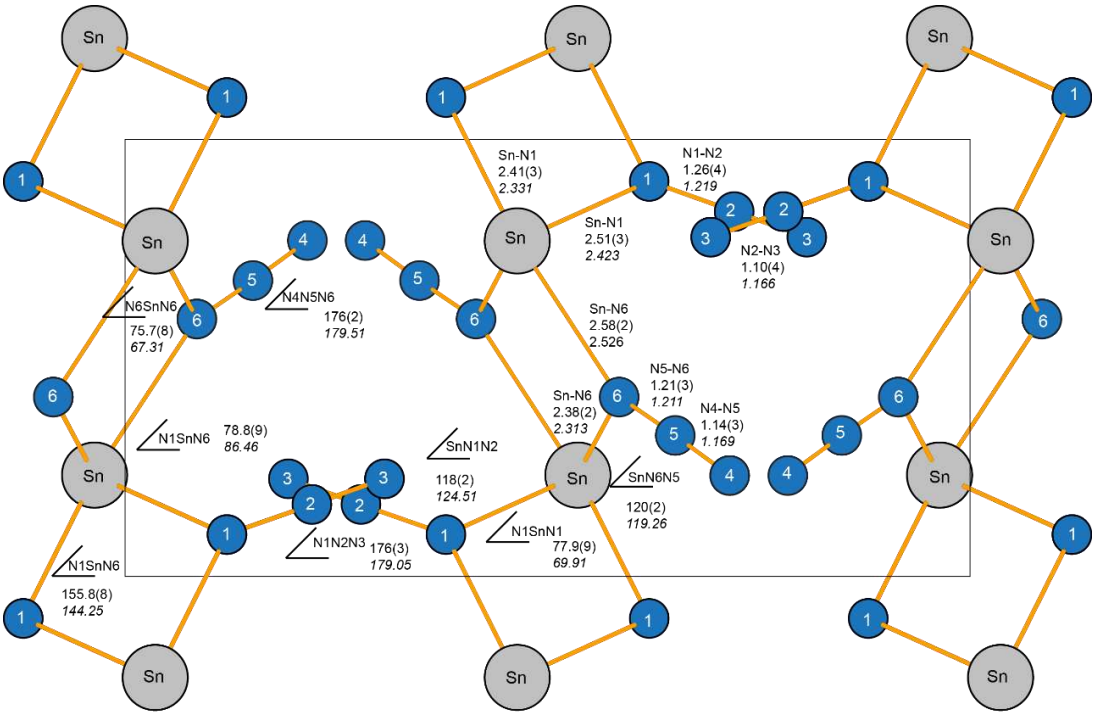

Figure 4. Projection down the crystallographic *a*-axis of the $Sn(N_3)_2$ structure (**1**) calculated by DFT-D methods. Parameters from refinement of XRD data are shown alongside italicised figures from calculated values. See also table 2.

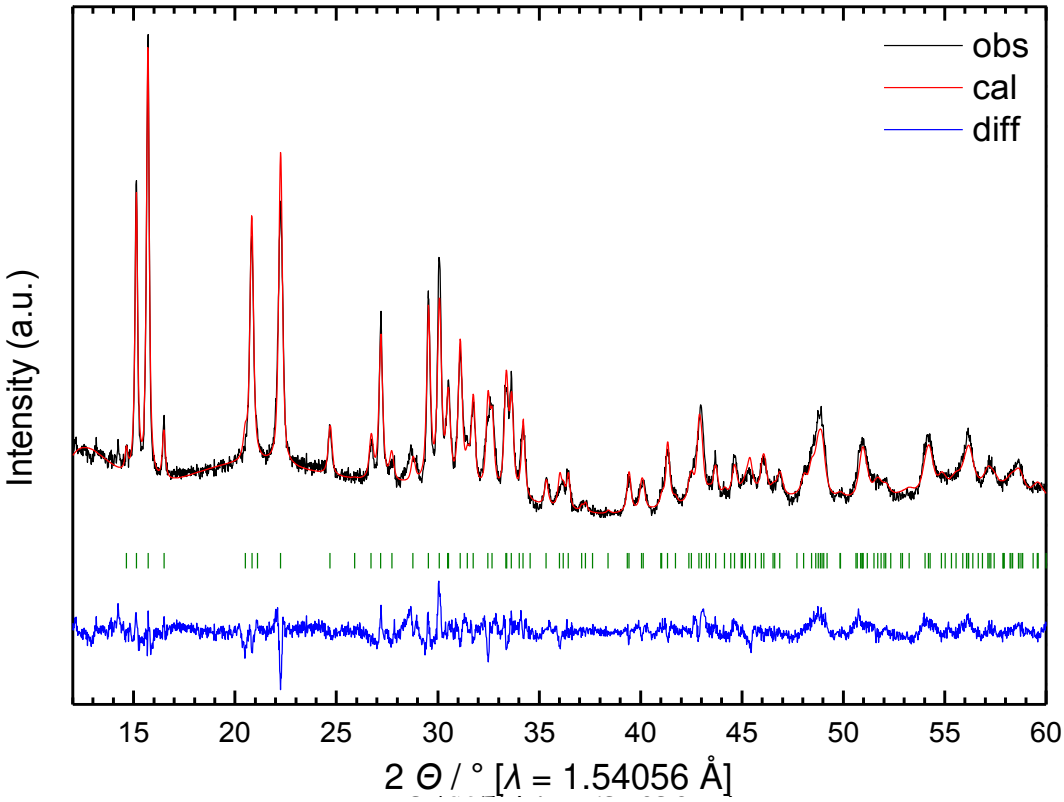

Figure 5. Overlay of observed (obs) and predicted (cal) PXRD patterns of **1**, and difference between observed and predicted intensities (diff) after final Rietveld refinement (R_{wp} = 6.751%, R_{exp} = 3.708%, R_p = 5.342%, GOF = 1.820.

Table 2. Molecular geometries and unit cell dimensions obtained from DFT-D calculations and from refinement of PXRD data.

	Distances / Å			Angles / °	
	DFT-D [a]	PXRD [b]		DFT-D [a]	PXRD [b]
N1–N2	1.219(-3.6)	1.26(4)	N1–Sn–N6	86.46(9.7)	78.8(9)
N2–N3	1.166(6.2)	1.10(4)	N1–Sn–N6^{i}	144.25(-7.4)	155.8(8)
N4–N5	1.169(2.0)	1.15(3)	N1–Sn–N1^{i}	69.91(-10.3)	77.9(9)
N5–N6	1.211(-0.3)	1.21(3)	N6–Sn–N6^{i}	67.31(-11.1)	75.7(8)
Sn–N1	2.331(-3.4)	2.41(3)	N1–N2–N3	179.05(1.9)	176(3)
Sn–N6	2.313(-2.8)	2.38(2)	N4–N5–N6	179.51(2.0)	176(2)
Sn···N1	2.423(-3.7)	2.51(3)	Sn–N1–N2	124.51(5.5)	118(2)
Sn···N6	2.526(-2.3)	2.58(2)	Sn–N6–N5	119.26(0.3)	120(2)
Sn···N4	2.787(-4.4)	2.916(19)	ΔNN	4.7	11.8

Unit cell parameters ($P2_1/a$, $Z = 4$)

	DFT-D	PXRD [b]
a / Å	6.7760	6.4463(7)
b / Å	11.0593	11.702(1)
c / Å	6.2327	6.0597(6)
β / °	94.671	94.239(6)
V / Å^3	465.51	455.86(16)

[a] deviation (%) from experimentally determined values given in parentheses [b] estimated standard deviations of experimental values given in parentheses.

The structure of compound **1** consists of the two crystallographically independent azido groups, N_3^1 (N1, N2, N3) and N_3^2 (N4, N5, N6), and of one type of independent Sn atoms. Each Sn is closely coordinated by four N_3 groups in a distorted disphenoidal geometry (Sn-N_α ax 2.42, 2.53 Å, N1-Sn-N6 144° and Sn-N_α eq 2.31, 2.33 Å, N1-Sn-N6 86°). Each N_3 group links two Sn centres *via* $\mu_{1,1}$ bridges (Sn-N1-Sn 110, Sn-N1-Sn 113°) and every Sn centre is linked to two adjacent Sn centres *via* two bridges each to form a folded, infinite zigzag coordination polymer chain that extends along the crystallographic *c*-axis (Fig. 4). Only one of the two crystallographically independent azido groups (N_3^2) interlinks these chains *via* $\mu_{1,3}$ bridges and comparably long Sn-N_γ bonds (2.79 Å), whereas the inter-chain interaction involving the N_3^1 groups (3.47 Å) is weak and has predominantly van-der-Waals character (d_{vdW}(Sn-N) *ca*. 3.7 Å). Unlike structures **2**-**4**, there are no terminal N_3 ligands. The structure of **1** contrasts that of its homologue, $Pb(N_3)_2$, in two ways. Firstly, Sn shows a coordination number of 4 whereas Pb is coordinated by eight azide ligands. Secondly, in **1** primarily only N_α participates in bridging unlike in $Pb(N_3)_2$ where both terminal N atoms of all azido groups are ligated

to Pb. A recent report on α-$Zn(N_3)_2$ revealed edge- and corner-sharing ZnN_4 tetrahedra forming a columnar structure whereas the presence of lone pairs at the coordination centre of tin prevent such a highly symmetrical three-dimensional arrangement in **1** (Fig. S5a). It is interesting to note that the unit cell volume per formula unit of **1** (114 Å^3) is approximately 12 Å^3 larger than that of orthorhombic $Pb(N_3)_2$ [6] (*Pnma*, 102 Å^3). Even though similar effects were observed in the EY_2 pairs SnF_2 (53.4 Å^3, *C*2/*c*),[48] PbF_2 (46.3 Å^3 orthorhombic, 52.4 Å^3 cubic)[49] and $SnCl_2$ (79.5 Å^3, *Pnam*),[50] $PbCl_2$ (78.1 Å^3, *Pnma*),[51] the volume increase is unusually large in **1**, which we assign largely to the fact that tin in SnF_2 is pentacoordinate, whereas in **1** the coordination number is unusually low (4), leading to a substantial decrease in the packing density.

Spectral properties

It is not possible to compare directly the IR spectral properties (see Table 4) in solution due to the insolubility of the new compounds in a common inert solvent. The most intense bands arising from the antisymmetric N_3 stretching vibrations, $\nu_{as}(N_3)$, appear in suspension between 2070 cm^{-1} (**1**) and 2060 cm^{-1} (**4**), which places the compounds within the range of the previously reported frequencies for Sn(II) azides but below those of the Sn(IV) complexes $Sn(N_3)_4(py)_2$ (2083 cm^{-1}) and $Sn(N_3)_6^{2-}$ (2083 cm^{-1}). The spectra of **2** and **3** in pyridine and picoline are nearly identical in the $\nu_{as}(N_3)$ range and display the doublet pattern expected for the *cis*-arrangement of the azido ligands with the band at higher energy having lower intensity. The absence of additional bands in this range strongly indicates that these complexes dissolve as monomers in the investigated solvents. Intriguingly, a comparison of the band maxima of the fundamental synchronous $\nu_{as}(N_3)$ vibrations (2060 cm^{-1}, **3**; 2055 cm^{-1}, **4**) shows the same trend that was found previously for the related Sn(IV) complexes $Sn(N_3)_4(py)_2$ (2083 cm^{-1}) and $Sn(N_3)_6^{2-}$ (2079 cm^{-1}) in the same solvent, which is caused primarily by electronic changes at the coordination centre upon exchanging azido for pyridine / picoline ligands. The effect of hydrogen bonding between anion and cation in **4** can be ascertained by comparison with a $Sn(N_3)_3^-$-containing compound with weakly-coordinating cations, $(PPh_4)Sn(N_3)_3$. In solid **4**, the $\nu_{as}(N_3)$ bands are broadened while in THF solution the peak maximum of the fundamental synchronous $\nu_{as}(N_3)$ stretch is shifted 5 cm^{-1} up. Finally, the $\nu_{as}(N_3)$ stretches of **1** are *ca.* 35 cm^{-1} above those of $(PPh_4)Sn(N_3)_3$ signalling a dramatically increased covalency of the Sn–N_α bonds in the former, although the effect is much smaller than, for example, in the related Si(IV) complexes $Si(N_3)_4$ (2170 cm^{-1}) *vs*. $Si(N_3)_6^{2-}$ (2109 cm^{-1}).[16]

Table 3. Comparison of solution and solid state FTIR spectra of azides **2**–**4** with the available literature data for Sn(II) azides.

	$\nu_{asym}(N_3)$ / cm^{-1}	$\nu_{sym}(N_3)$ / cm^{-1}	medium	ref.
$Sn(N_3)_2$ (**1**)	2107, 2090, 2070	1339, 1333, 1286, 1276	nujol	this paper

$Sn(N_3)_2(py)_2$ (**2**)	2065	1326	nujol	this
	2077, 2057	1325	pyridine	paper
$Sn(N_3)_2(pic)_2$ (**3**)	2063, 2041	1321	nujol	this
	2076, 2057	1324	4-picoline	paper
	2082, 2060	1324	MeCN	
$(G)Sn(N_3)_3$ (**4**)	2060, 2034	1332	nujol	this
	2086, 2056	1323	MeCN	paper
	2081, 2055	1320	THF	
$\{(^nPr)_2ATI\}SnN_3$	2039	1308	KBr	[19]
	2051	-	toluene	
$(Tp^{CF3}Ag)Sn(N_3)\{(^nPr)_2ATI\}$	2070	-	KBr	[20]
$\{(Mes)_2DAP\}SnN_3$	2060	1310*	KBr	[21]
$HC(PPh_2{=}NSiMe_3)_2SnN_3$	2048	-	KBr	[24]
$(PPh_4)Sn(N_3)_3$	2069, 2060, 2034	1320	Nujol	[25]
	2081, 2073, 2050	-	THF	

* $\nu_{sym}(N_3)$ cannot be assigned unambiguously due to presence of multiple peaks in region; Tp^{CF3} = hydrotris{3,5-bis(trifluoromethyl)pyrazolyl)borate}.

The findings of the IR spectral investigation are consistent with the NMR spectra of compounds **2**-**4** (Table 4). While ^{14}N chemical shifts are insensitive to changes in the ligand sphere for complexes of which data are available, those of ^{119}Sn decrease dramatically upon increasing the coordination number from 3 (above –300 ppm, compound **4** and the previously published data) to 4 (compound **2** and **3**, below –300 ppm).

Table 4. ^{14}N and ^{119}Sn NMR chemical shifts of compounds **2–4** with available literature data.

NMR δ / ppm	^{14}N				^{119}Sn	solvent	ref.
Compound	N_α	N_β	N_γ	N_L			
$Sn(N_3)_2(py)_2$ (**2**)	–258.7	–135.1	*a*	–62.9	–459.2	C_5D_5N	*b*
$Sn(N_3)_2(pic)_2$ (**3**)	–260.4	–135.2	*a*	–62.6 *c*	–458.7	C_5D_5N	*b*
$(G)Sn(N_3)_3$ (**4**) *d*	–260.1	–136[a]	–217.1	*e*	–284.8	CD_3CN	*b*
$(PPh_4)Sn(N_3)_3$	–260.0	–136[a]	–218.5	*e*	–220	CD_3CN	[25]
$\{(Mes)_2DAP\}SnN_3$	–292	–136	–223	-	–276.2	CD_2Cl_2	[21]
$\{(^nPr)_2ATI\}SnN_3$	–256	–136	–217	–202	–122.4	CD_2Cl_2	[19]
$HC(CMeNPh)_2SnN_3$	-	-	-	-	–156.2	$CDCl_3$	[22]
$HC(PPh_2{=}NSiMe_3)_2SnN_3$	-	-	-	-	–199.8	THF-d_8	[24]
$HC(CMeNAr)_2SnN_3$ *f*	-	-	-	-	–237	C_6D_6	[23]
$(L_3Ag)SnN_3\{(n\text{-}Pr)_2ATI\}$ *g*	-	-	-	-	90	-	[20]

[a] Not observed, [b] this paper, [c] obscured by solvent peak, [d] G = $C(NH_2)_3$, [e] not applicable, [f] Ar = *i*-$Pr_2C_6H_3$, [g] L_3 = hydrotris(3,5-bis(trifluoromethyl)pyrazolyl)borate.

Thermal Properties

Heating of **3** in a standard melting point capillary shows complete melting at 101 °C, condensation above the melt and explosion of the sample upon further heating leaving behind fine black soot. According to differential scanning calorimetry (DSC, Fig. 6, left; Table 5) measurements, both **2** and **3** have sharp melting points (T_{on}^{m} = 62 °C and 100 °C, respectively), 80 to 90 K above which strongly exothermic decomposition sets in (T_{on}^{dec} / °C = 172(±3), **2**; 180(±3), **3**). While the exotherm of the pyridine adduct (**2**) is sharp (T_{max} = 190 °C), the picoline adduct (**3**) requires much higher temperatures (up to 280 °C) to undergo complete decomposition. Despite this, the integrated molar heats of decomposition are similar for both adducts (ΔH_{dec} / (kJ mol^{-1}) = –369(±26), **2**; –416(±17) kJ mol^{-1}, **3**; Fig. 6, left).

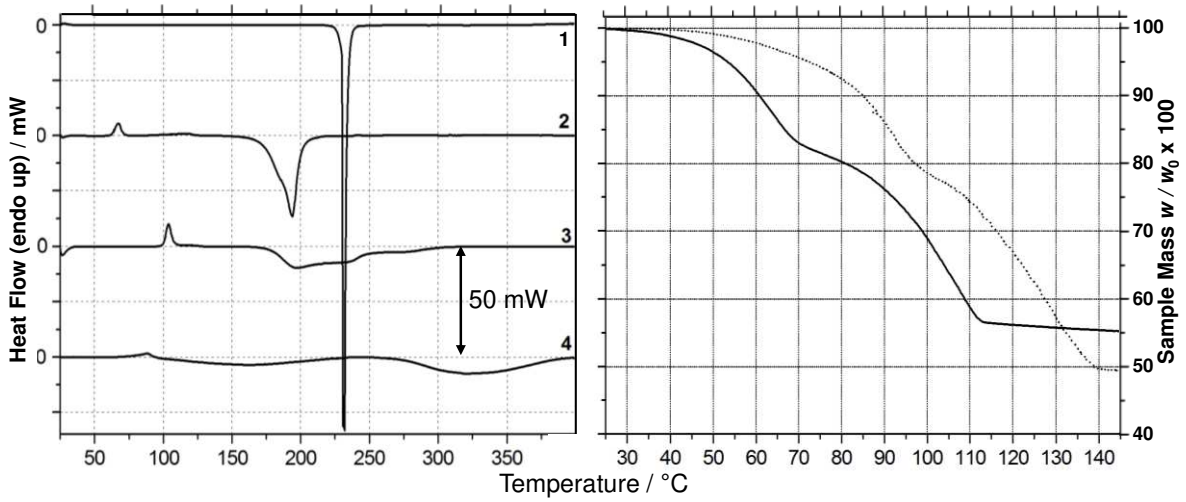

Figure 6. Thermogram series of $Sn(N_3)_2$ (**1**) , $Sn(N_3)_2(py)_2$ (**2**), $Sn(N_3)_2(pic)_2$ (**3**) and $C(NH_2)_3Sn(N_3)_3$ (**4**) (DSC in sealed capsules, left) and **2** (—) and **3** (···) (TGA, right); heating rate 10 K min^{-1}.

Guanidinium triazidostannate (**4**) also has a low melting point (approximately 77 °C, followed immediately by two broad exotherms (T_{on}^{dec} / °C = 95(4), 272(2) °C; ΔH_{dec} / (kJ mol^{-1}) = –234(±5), –401(±14)). Both melting and decomposition onset temperatures for **3** are below that of $(PPh_4)Sn(N_3)_3$ suggesting the involvement of the guanidinium cation in the initial thermolysis step. Tin diazide (**1**), on the other hand, neither melts nor undergoes any phase change before detonation, which occurred upon heating (10 K min^{-1}) of two samples to 230 and 250 °C, respectively; Fig. S33. All heat release curves follow patterns found in the Sn(IV) polyazido compounds were each azido ligand contributed –208(±7) kJ mol^{-1} [12] to ΔH_{dec} (Sn(II) polyazides: –185(±13) kJ mol^{-1} (**1**) to 212 (±6) kJ mol^{-1} (**4**)) (Table 5). Crucially, however, the decomposition of the Sn(II) polyazides begins at considerably lower temperatures (95 to 230 °C) than their Sn(IV) analogs (265 to 305 °C). On the N_2-purged thermobalance, the adducts undergo two mass loss steps at T_{on} / °C = 48, 83 (**2**), and 75, 111 (**3**) (Fig.

6, right) that correspond to the loss of stoichiometric amounts of pyridine or picoline starting at temperatures below the onset of the first endothermic processes observed in the DSC using sealed stainless steel capsules. The observed mass losses of 44% and 50% correspond well with two molar equivalents of pyridine (44%, **2**) or picoline (48%, **3**), both leaving behind **1** (temperatures were kept below 150 °C to prevent damage to the balance, Figure 6, right). This is corroborated by TOF-MS-AP^+ mass spectrometry data for solid **3** which shows the release of 4-picoline by the dominant signal at m/z = 186 amu. (twice the mass of the ligand).

Table 5. DSC onset temperatures and enthalpies [a] of $Sn(N_3)_2$ (**1**), $Sn(N_3)_2(py)_2$ (**2**), $Sn(N_3)_2(pic)_2$ (**3**) and $(G)Sn(N_3)_3$ (**4**)

	1	**2**	**3**	**4**
T_{on}^{m} / °C [b]	-	62.4(2)	99.9(5)	77.3(1)
ΔH_m / (kJ mol^{-1})	-	20.0(3)	28.8(9)	7.81(9)
T_{on}^{dec} / °C [b]	>230 [c]	172(3)	180(3)	95(4), 272(2)
ΔH_{dec} / (kJ mol^{-1})	–372 [d]	–369(26)	–416(17)	–234(5), –401(14)
ΔH_{dec} / (kJ g^{-1})	–1.84 [d]	–1.0(1)	–1.07(4)	–0.77(2), –1.32(5)

[a] estimated errors shown in parentheses, [b] Extrapolated onset temperature, [c] lowest of two measurements, [d] lower bound due to instrument-specific truncation of range-exceeding signal.

Conclusions

A type of low-valent polyazido tin compounds has been discovered in reactions of tin(II) fluoride with trimethylsilyl azide in polar coordinating reaction solvents. These compounds consist of well-defined tetracoordinate complexes that can be regarded as Lewis acid-base adducts of $Sn(N_3)_2$ with pyridine (**2**) or 4-picoline (**3**) as sterically not very demanding electron donors. Both adducts are stable at r.t. under a static atmosphere and exhibit no noticeable sensitivity toward friction or impact, but de-coordinate solvent by two-step processes at slightly elevated temperatures under a dynamic atmosphere. This characteristic is essential in achieving the fast, facile and safe method of preparing tin(II) azide, $Sn(N_3)_2$ (**1**), from insensitive starting material under non-cryogenic conditions that this paper demonstrates. $Sn(N_3)_2$ is a colourless explosive solid of greater sensitivity than $Pb(N_3)_2$. Azide **1** proved to be suitable as a reactive starting material in the preparation of tin(II) azido complexes, including guanidinium triazidostannate(II). All investigated tin(II) polyazides have a marked air sensitivity, low thermal stability and oxidise readily to their tin(IV) analogues in the presence of ethereal HN_3. Their structures are dominated by comparably long, polar, coordinative Sn-N bonds, stereochemically active lone electron pairs and, as a consequence of their coordinatively unsaturated nature, engage in extensive directed intermolecular interaction, effectively leading to dimeric or polymeric assemblies. The presence of guanidinium cations as hydrogen bond-donors gives rise to an extensive hydrogen bond network between anions and cations of $\{C(NH_2)_3\}Sn(N_3)_3$ (**4**) that may

contribute towards the stabilisation of the nitrogen rich (55 % N) compound, and its apparent low sensitivity toward friction and impact.

Experimental Section

CAUTION: Tin(II) azide is a highly sensitive and explosive powder. It should be made and handled on a small scale only, with suitable safety precautions in place (face shield, gloves, ear plugs and protective clothing). Synthetic procedures were performed using standard Schlenk, vacuum line, and glovebox techniques under an atmosphere of dry and oxygen-fee argon. The typical ultimate vacuum was close to 4×10^{-2} mbar. Samples used for analytical examination were prepared in the glovebox whenever possible. Filtration of air- and / or moisture-sensitive compounds was achieved by the use of stainless steel filter cannulas equipped with glass fibre filters secured by PTFE tape. MeCN (Fisher, 99.9 %), and MeCN-d_3 (Aldrich, 99.8 %), 4-picoline (Aldrich, 98 %), pyridine (Fisher Scientific, 99.8 %), and pyridine-d_5 (Sigma Aldrich, 99.5 %) were dried over CaH_2 (Acros, 93 %) for 18 h before either trap-to-trap condensation or vacuum distillation. Solvents were degassed and then stored under an Ar atmosphere in glass ampoules and sealed by J. Young's high vacuum greaseless stopcocks. TMS–N_3 was prepared according to a published procedure.[[42, 43]52, 53] SnF_2 (99 %) and $SnCl_2{\cdot}2H_2O$ (98 %, both Sigma Aldrich,) were vacuum-dried at 110 °C for 16 h. All dried solid reagents were stored in sealed vessels in a glovebox. Infrared absorption spectra in the range 500–4000 cm^{-1} were recorded on a Bruker Tensor 27 FTIR or Alpha FTIR spectrometers running *Bruker OPUS 7.0* software, at a spectral resolution of 2 cm^{-1}, using samples either as nujol mull between NaCl windows or in solution contained in a Specac CaF_2 cell (spectra Figs. S6-S13). The abbreviations vs, very strong; s, strong; m, medium; w, weak; vw, very weak; sh, shoulder; br are used to indicate the relative absorbance of bands in IR spectra. Elemental analyses were carried out by the University of Sheffield elemental analysis service on a PerkinElmer 2400 CHNS/O series II elemental analyser in an atmosphere of pure oxygen. ^{1}H and ^{13}C NMR spectra were recorded using a 400 MHz Bruker Avance 400 spectrometer; ^{14}N and ^{119}Sn spectra were recorded on a 500 MHz Bruker Avance 500 spectrometer. NMR spectra are calibrated against the residual solvent peak (^{1}H) and solvent peak (^{13}C) according to ref. [54] or $SnMe_4$ (^{119}Sn) and were processed using *Bruker TOPSPIN v3.2* (spectra Figs. S14-S26). DSC measurements were performed on a PerkinElmer Pyris 1 differential scanning calorimeter (DSC) operated under a flow of N_2 (20 ml min^{-1}) with a heating rate of 10 K min^{-1}. The instrument was calibrated against a reference of pure In (99.999 %) using the transition at 156.60 °C (28.45 J g^{-1}). DSC samples were hermetically sealed in PerkinElmer stainless steel high-pressure capsules (30 μL internal volume) with Au-plated Cu seals (T_{max} = 400 °C, p_{max} = 150 bar). Thermogravimetric analyses (TGA) were carried out using a Pyris 1 thermogravimetric analyser with a heating rate of 10 K min^{-1} under a flow of N_2 (20 ml min^{-1}). Onset temperatures (T_{on}), mass losses, enthalpies of fusion (ΔH_{fus}), and decomposition (ΔH_{dec}) were determined using the data analysis tools within the *Pyris 1* software (thermographs Figs. S27-S34). Caution! A 1.4 mg sample of compound **1** ruptured the base

of the stainless steel DSC sample capsule (Fig. S33, inset) causing deformation of the heating stage platinum cover. No further measurements were performed on this substance. Single crystals were obtained by slow cooling of saturated solutions to −19 °C overnight in pyridine (**2**), picoline (**3**) and MeCN (colourless needles of **4**). Single crystal X-ray diffraction (XRD) measurements were carried out using graphite-monochromated Mo $K_{\alpha 1,2}$ radiation (λ = 0.71073 Å) at 100 K on a Bruker SMART 4000 diffractometer equipped with a CCD area detector and an Oxford Cryosystems Cobra cryocooler. Data were collected using Bruker *APEX2* (2012) software and integrated using Bruker *SAINT* (2007) absorption correction was applied using Siemens' Area Detector Absorption correction (*SADABS,* G. M. Sheldrick, 2007). All structures were solved using direct methods for the location of heavy atoms and refined using (*SHELXS-97* within *SHELXTL-2013* and *SHELXL-2014*, G. M. Sheldrick, 1997),[55] C-bound hydrogen atom positions were calculated and refined using a riding model with isotropic displacement parameters of $1.2U_{eq}$ of the parent atom, whereas those bound to N were located *via* the Fourier difference map, and refined freely. Additional twin refinement was carried out for **2** using the twinning tools within *WinGX*,[56, 57] which gave a modest improvement in structure quality that reduced *R*1 from 6.3 % to 4.5%. Thermal ellipsoid structure plots were generated using the POV-ray interface within *Mercury 3.8* (ccdc.cam.ac.uk). During the crystal screening stage, use of anhydrous nujol (stored over Na) was essential to protect the crystals until mounted in the nitrogen stream. Non-dry nujol led to the formation of gas bubbles emanating from the crystals. Powder X-ray diffraction data were collected for a sample of $Sn(N_3)_2$ carefully loaded into a 0.7 mm borosilicate glass capillary prior to being mounted and aligned on a Bruker-AXS D8 Advance powder diffractometer operating with Ge-monochromated Cu $K_{\alpha 1}$ radiation (λ = 1.54056 Å). Powder patterns were measured and baseline-corrected using the Bruker *DIFFRAC.EVA* software suite (v3.1, Bruker, 2010). A Pawley refinement[58] was implemented to index the powder pattern using *TOPAS* (A. A. Coelho, 2007). Structure optimizations were performed using density functional theory plus dispersion (DFT-D) and the plane-wave pseudopotential method as implemented in *CASTEP* version 16.1 [59] utilizing the dispersion correction scheme of Tkatchenko and Scheffler.[60] Treatment of electronic exchange and correlation was handled by the generalized gradient approximation (GGA) as formalised by Perdew, Burke and Ernzerhof (PBE). The density mixing scheme of Pulay was implemented with mixing amplitude (0.5), maximum g-vector (1.5 $Å^{-1}$), number of extra bands (14), smearing scheme (Gaussian) and smearing width (0.1 eV) as indicated.[61] On-the-fly (OTF)[62] pseudopotentials were generated using the CASTEP code; the plane-wave cut-off energy used throughout was 950 eV, which ensured convergence of both lattice parameters and total energies (to less than 0.002 meV per atom). Brillouin zone sampling was obtained using a Monkhorst-Pack[63] grid of 3 × 2 × 4 (spacing < 0.5 $Å^{-1}$, 5 k points). The structures were relaxed using the Broyden, Fletcher, Goldfarb and Shannon (BFGS)[64] method in order to allow for both atomic coordinates and unit cell vectors to optimize simultaneously while constraining space group geometry (convergence criteria: maximum change in system energy equal to 5×10^{-6} eV, maximum root-mean-square (RMS) force =

0.01 eV $Å^{-1}$, maximum RMS stress = 0.01 GPa and maximum RMS displacement equal to 5×10^{-4} Å).

Preparation of diazidobis(pyridine)tin(II) (2) from SnF_2

TMS–N_3 (442 mg, 3.84 mmol, 2.5 eq.) was added dropwise to a stirred suspension of SnF_2 (241 mg, 1.54 mmol) in pyridine (8 ml). The mixture was stirred at r.t. for a total of 16 h. Within the first 0.5 h the mixture became gradually clearer. The resultant, slightly turbid solution was filtered into a Schlenk tube and the clear filtrate concentrated to a volume of *ca.* 2 ml upon which a crystalline precipitate formed. The precipitate was re-dissolved by warming the vessel to 35 °C in a water bath, and crystallisation from the now pale yellow solution was induced by cooling to –19 °C overnight. The supernatant solution was decanted, and the crystals were dried in a stream of argon until the mass remained constant (*ca.* 5 mins) to afford 363 mg of **2** (65 % based on SnF_2). No satisfactory elemental analyses (360.81 g mol^{-1}) could be obtained due to rapid pyridine loss even at r.t. and great sensitivity to moisture. FTIR (nujol) ν / cm^{-1} = 3361w, 3315w, 3106vw, 3095w, 3072vw, 3058vw, 3035w, 3022w, 3000w, 2596w, 2066vs, 1945vw, 1869vw, 1640w, 1602s, 1573w, 1486m, 1448s, 1396w,br, 1360vw, 1324s, 1276s, 1247vw, 1216vw, 1194vw, 1157vw, 1064m, 1035, 1009, 755m, 700m, 652w, 645vw, 628m, 599w; pyridine: 2077s, 2057vs, 1325w,br, 1272vw,br. NMR (pyridine-d_5) $\delta(^1H)$ / ppm = solvent only: 7.22 (m, 2H), 7.59 (m, 1H), 8.74 (m, 2H); $\delta(^{13}C)$ / ppm = 124.09 (t, C_5D_5N), 124.63 (s), 136.15 (t, C_5D_5N), 136.64 (s), 150.35 (t, C_5D_5N), 150.76 (s); $\delta(^{14}N)$ / ppm = –62.92 (pyridine-d_5, $\Delta\nu$ = 363 Hz), –258.71 (N_α, $\Delta\nu$ = 335 Hz), –135.1 (N_β, $\Delta\nu$ = 52 Hz); $\delta(^{119}Sn)$ / ppm = –459.2 ($\Delta\nu$ = 120 Hz). DSC T_{on} / °C = 62.4(2) (melting), T_{on} = 172(3) (decomposition), ΔH_{dec} = −369(29) kJ mol^{-1}, –1.02(8) kJ g^{-1}. N.B. drying under dynamic vacuum for > 1 h causes disintegration of the crystals, giving $Sn(N_3)_2(py)_{(2-x)}$ and eventually $Sn(N_3)_2$. Storing the solid in a sealed vial in the glovebox inhibited pyridine loss.

Preparation of 2 from $SnCl_2$

$SnCl_2$ (365 mg, 1.92 mmol) was suspended in pyridine (15 ml, 0.19 mol), and NaN_3 (2.601 g, 40.0 mmol, *ca.* 21 eq.), was added and the resulting mixture stirred for 16 h at r.t. A FTIR spectrum of the solution exhibited at this stage the following bands assigned to azide groups: $\nu(N_3)$ / cm^{-1} = 2076vw,sh, 2069vs, 2057w,sh, $\nu(N_3)_{sym}$ / cm^{-1} = 1324m, 1272w. The suspension was then filtered and the filtrate collected in a new Schlenk tube containing a second batch of NaN_3 (3.98 g, 61.2 mmol, *ca.* 32 eq.). This mixture was stirred for a further 16 h. At this stage, the IR spectrum of a diluted sample resembled that of a genuine sample of compound **2** prepared *via* the SnF_2 and TMS-N_3 route, except for a small shoulder at 2068 cm^{-1} which could be due to a trace of $SnCl(N_3)(py)_2$ from incomplete N_3/ Cl exchange. FTIR (pyridine) ν / (cm^{-1}) = 2076s, 2069vw,sh, 2057vs, 1324m, 1273w. The same work-up procedure was used for **3** as for the above preparation affording compound **3** in a comparable yield.

Tin(II) azide, $Sn(N_3)_2$ (1)

*Caution: Tin(II) azide is highly explosive and very sensitive to impact, friction and electrostatic discharge. Slightest scratching action or touching the substance with ungrounded equipment will cause detonation. Appropriate additional personal protective equipment (PPE) must be applied during manipulations, including full face-shield, Kevlar gloves, and anti-static wristband. The use of Teflon-coated spatulas is recommended for transferal of material between vessels. Compound **1** can be phlegmatised in a mull with paraffin.*

Dry MeCN (10 ml) was added to $Sn(N_3)_2(py)_2$ (**2**, 118 mg, 0.327 mmol) forming a fine white suspension, which was stirred vigorously for 2 h. The mixture was then allowed to settle, the supernatant solution was decanted, and the off-white decantation residue carefully dried under vacuum for 1 h at r.t. to afford 42 mg (η = 63 %) of compound **1** (202.73 g mol^{-1}). FTIR (nujol) ν / (cm^{-1}) = 3380vw, 3325vw, 2613vw, 2593vw, 2554vw, 2536vw, 2107sh, 2090sh, 2070vs, 1339m, 1333m, 1286m, 1276m, 1184vw, 1177vw, 659m, 594w, 591w. See SI for PXRD data.

Diazidobis(4-picoline)tin(II) (3)

TMS–N_3 (294 mg, 2.56 mmol, *ca.* 2.5 eq.) was added dropwise over 1 minute to a stirred suspension of SnF_2 (162 mg, 1.03 mmol) in 4-picoline (5 ml). The mixture was stirred for 16 h at RT before a small amount of insoluble material was removed by filtration. The clear, pale yellow filtrate was then concentrated under vacuum until the onset of crystallization occurred, after which it was slowly cooled to −19 °C overnight giving **3** as colourless, rod-shaped crystals. The melting point of 4-picoline is *ca*. 2 °C. Occasionally, the crystallisation solution froze, but once thawed the supernatant pale yellow supernatant solution was readily decanted from the crystalline $Sn(N_3)_2(pic)_2$. The crystals were dried under dynamic vacuum until the mass remained constant (*ca.* 0.5 h) to afford 308 mg of **3** (η = 77 % based on SnF_2). Elem. anal. (%) for $C_{12}H_{14}N_8Sn$, $Sn(N_3)_2(pic)_2$, 389.01 g mol^{-1}, calcd.: C 37.05, H 3.63, N 28.80; for $Sn(N_3)_2(pic)_{1.904}$: C 36.10, H 3.53, N 29.13; found: C 36.00, H 3.21, N 28.72. FTIR (nujol) ν / cm^{-1} = 3400vw, 3380vw, 3349s, 3308m, 3291vw,sh, 3233vw, 3223vw, 3121w, 3078vw, 3060vw, 3047vw, 3027vw, 2743vw, 2678vw, 2662vw, 2646w, 2636vw,sh, 2597m, 2534w, 2493w, 2487w, 2433vw, 2419vw, 2400w, 2371vw, 2352vw, 2326vw, 2317vw, 2310vw, 2233w, 2226vw, 2183vw,sh, 2172vw,sh, 2063vs,br, 2041s, 1979w,sh, 1959w,sh, 1937w,sh, 1853w, 1770vw, 1687m, 1620vw, 1612s, 1560m, 1456w, 1321m, 1271m, 1243w, 1227m, 1216w, 1204m, 1118m, 1100m, 1067s, 1045m, 1014s, 1007s, 979m, 970w, 959w, 878m, 807vs,br, 667w, 649m, 641m, 604m, 537m, 526m, 518w; $Sn(N_3)_2(pic)_2$ in 4-picoline: 2076s, 2057vs, 1324w,br, 1273vw,br. NMR (pyridine-d_5) δ (^{1}H) / ppm = 2.12 (s, 6H) 7.04 (d, 4H) 8.62 (dd, 4H); δ (^{13}C) / ppm = 21.13 (s), 125.51 (s), 147.69 (s), 150.47 (s); δ(^{14}N) / ppm = –62.62 (pyridine-d_5, $\Delta\nu$ = 292 Hz), 135.2 (N_β, $\Delta\nu$ = 49 Hz), –260.4 (N_α, $\Delta\nu$ = 280 Hz); δ(^{119}Sn) / ppm = –458.74. DSC T_{on} / °C = 99.9(5) (melting), T_{on} = 180(3) (decomposition), ΔH_{dec} = −416(17) kJ mol^{-1}, –1.07(4) kJ g^{-1}.

Direct preparation of guanidinium tri(azido)stannate(II) (4) from SnF_2, TMS–N_3 and (G)N_3

TMS–N_3 (315 mg, 2.74 mmol) was added dropwise over 1 minute to a stirred suspension of SnF_2 (328 mg, 2.09 mmol), and anhydrous guanidinium azide (236 mg, 2.31 mmol) in CH_3CN (15 ml). The mixture was stirred for 1.5 h giving a white suspension, which was filtered and the filter residue residue extracted with CH_3CN (20 ml). The combined filtrate and extraction solutions were concentrated to a volume of *ca*. 5 ml, and cooled to –19 °C overnight which induced crystallisation. In the cold, the supernatant solution was then decanted from the white microcrystalline solid, and the solid dried under vacuum at *ca*. 45 °C for 10 minutes which afforded 368 mg of compound **4** (304.79 g mol^{-1}, η = 58 % based on SnF_2). FTIR (nujol) ν / (cm^{-1}) = 3460wsh, 3434sbr, 3405vsbr, 3337wsh, 3237sbr, 3168vsbr, 2071wsh, 2060vsbr, 2034sbr, 1659vsbr, 1332m, 1283m, 1262wsh, 1009vw, 654m, 600w; CH_3CN: 3457mbr, 3367mbr, 3282mbr, 3215mbr, 2086s, 2056vs, 1670m, 1323wbr, 1275vwbr; THF: 3350m,br, 3172m,br, 2081s, 2055vs, 1668m, 1582vw, 1321w, 1279w. NMR (400 MHz, CD_3CN) δ (^{1}H) / ppm = 6.11; δ (^{13}C) / ppm = 159.0; δ (^{14}N) / ppm = –217.1, –260.1; δ (^{119}Sn) / ppm = –284.8 ppm. Note: due to extreme air sensitivity of solid **4**, attempts at elemental analysis were unsuccessful.

Preparation of 4 from 1

A Schlenk tube was charged with $Sn(N_3)_2$ (60 mg, 0.38 mmol), which was prepared as described above, and with guanidinium azide (38 mg, 0.37 mmol) and MeCN (20 ml). The resultant suspension was stirred rapidly and gradually became clear over a period of time of 20 minutes to form a colourless solution. This solution was stirred further for 2 h at r.t. before an IR spectrum of the solution was recorded, which confirmed the presence of guanidinium triazidostannate (**4**). Compound **4** crystallises from the reaction solution after its volume had been reduced to *ca.* 1 ml under vacuum upon cooling to –19 °C overnight. The identity of the compound obtained by this method was confirmed by an IR spectrum of a nujol suspension. With the exception of traces of TMS-N_3, the solution IR spectra (MeCN) of products obtained by both preparative methods are identical.

Associated Content

Crystallographic data for this paper (**1**, 433812; 1529432, **2**; 1529433, **3** and 1529434, **4**) can be obtained free of charge from the FIZ Karlsruhe or The Cambridge Crystallographic Data Centre *via* www.ccdc.cam.ac.uk/structures. The Supporting Information is available free of charge on the ACS Publications website at DOI: xxx containing diagrams and spectra as described in the text.

Acknowledgements

J. Gallant, S. Bradshaw, E. Carrington, T. Roseveare (powder X-ray and NMR measurements, preparative work). PP and RMC thank the University of Sheffield for funding.

Table of Contents Synopsis and Graphic

$Sn(N_3)_2(py)_2$ and $Sn(N_3)_2(pic)_2$ form upon reaction of tin(II) precursors with Me_3SiN_3 as tetracoordinate Lewis base adducts of $Sn(N_3)_2$. Solid $Sn(N_3)_2(py)_2$ de-coordinates pyridine reversibly and releases microcrystalline $Sn(N_3)_2$. The friction sensitive $Sn(N_3)_2$ reacts with a H-bond donor to form the salt-like and comparably stable guanidinium compound $\{C(NH_2)_3\}Sn(N_3)_3$ (55% N *w*/*w*). The polyazides are characterised by spectroscopic, thermochemical and crystallographic methods. $Sn(N_3)_2$ ($P2_1/a$) features tetracoordinate tin and differs dramatically from its well-known Pb analogue.

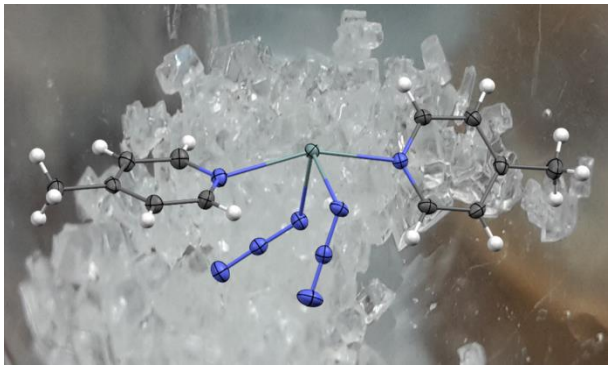

References

(1) Fehlhammer, W. P.; Beck, W. Azide Chemistry - An Inorganic Perspective, Part I, Metal Azides: Overview, General Trends and Recent Developments. *Z. Anorg. Allg. Chem.*, **2013**, *639*, 1053-1082.
(2) Fehlhammer, W. P.; Beck, W. Azide Chemistry – An Inorganic Perspective, Part II, [3+2]-Cycloaddition Reactions of Metal Azides and Related Systems. *Z. Anorg. Allg. Chem.* , **2015**, *641*, 1599-1678.
(3) Scriven, E. F. V.; Turnbull, K. Azides - Their Preparation and Synthetic Uses. *Chem. Rev.*, **1988**, *88*, 298-368.
(4) Portius, P.; Davis, M. Recent Developments in the Chemistry of Homoleptic Azido Complexes of the Main Group Elements. *Coord. Chem. Rev.*, **2013**, *257*, 1011-1025.
(5) Azaroff, L. V. Structural Investigation of Lead Azide. *Z. Kristallog. – Cryst. Mater.*, **1956**, *107*, 362-369.
(6) Choi, C. S.; Prince, E.; Garrett, W. L. Refinement of alpha-Lead Azide by Neutron Diffraction. *Acta Crystallogr. Sect. B*, **1977**, *B33*, 3536-3537.
(7) Müller, U. Crystal Structure Refinements of Potassium, Rubidium, Cesium, and Thallium Azides. *Z. Anorg. Allg. Chem.*, **1972**, *392*, 159-166.
(8) Lyhs, B.; Jansen, G.; Bläser, D.; Wölper, C.; Schulz, S. Synthesis and Structural Characterization of Antimony Polyazides. *Chem. Eur. J.*, **2011**, *17*, 11394 - 11398.
(9) Schulz, S.; Lyhs, B.; Jansen, G.; Bläser, D.; Wölper, C. Syntheses and Structures of Triazides of Heavy Group 15 Elements. *Chem. Commun.*, **2011**, *47*, 3401-3404.
(10) Haiges, R.; Boatz, J. A.; Vij, A.; Vij, V.; Gerken, M.; Schneider, S.; Yousufuddin, M.; Christe, K. O. Polyazide Chemistry. Preparation and Characterization of $As(N_3)_5$, $Sb(N_3)_5$, and $[P(C_6H_5)_4][Sb(N_3)_6]$. *Angew. Chem. Int. Ed.*, **2004**, *43*, 6676-6680.
(11) Haiges, R.; Rahm, M.; Dixon, D. A.; Garner, E. B.; Christe, K. O. Binary Group 15 Polyazides. Structural Characterization of $[Bi(N_3)_4]^-$, $[Bi(N_3)_5]^{2-}$, $[bipy{\cdot}Bi(N_3)_5]^{2-}$, $[Bi(N_3)_6]^{3-}$, $bipy{\cdot}As(N_3)_3$, $bipy{\cdot}Sb(N_3)_3$, and $[(bipy)_2{\cdot}Bi(N_3)_3]_2$ and on the Lone Pair Activation of Valence Electrons. *Inorg. Chem.*, **2012**, *51*, 1127-1141.

(12) Haiges, R.; Deokar, P.; Christe, K. O. Coordination Adducts of Niobium(V) and Tantalum(V) Azide $M(N_3)_5$ (M = Nb, Ta) with Nitrogen Donor Ligands and their Self-Ionization. *Angew. Chem. Int. Ed.*, **2014**, *53*, 5431-5434.
(13) Haiges, R. D., Piyush; Christe, Karl O. Adduct Formation of Tantalum(V)- and Niobium(V) Fluoride with Neutral Group 15 Donor Ligands, an Example for Ligand Induced Self-Ionization *Z. Anorg. Allg. Chem.*, **2014**, *640*, 1568-1575.
(14) Haiges, R.; Vasiliu, M.; Dixon, D. A.; Christe, K. O. The Uranium(VI) Oxoazides $[UO_2(N_3)_2 \cdot CH_3CN]$, $[(bipy)_2(UO_2)_2(N_3)_4]$, $[(bipy)UO_2(N_3)_3]^-$, $[UO_2(N_3)_4]^{2-}$, and $[(UO_2)_2(N_3)_8]^{4-}$ *Chemistry - A European Journal* **2017**, *23*, 652-664.
(15) Filippou, A. C.; Portius, P.; Neumann, D. U.; Wehrstedt, K.-D. The Hexaazidogermanate(IV) Ion: Syntheses, Structures, and Reactions. *Angew. Chem. Int. Ed.*, **2000**, *39*, 4333-4336.
(16) Filippou, A. C.; Portius, P.; Schnakenburg, G. The Hexaazidosilicate(IV) Ion: Synthesis, Properties and Molecular Structure. *J. Am. Chem. Soc.*, **2002**, *124*, 12396-12397.
(17) Campbell, R.; Davis, M. F.; Fazakerley, M.; Portius, P. Taming Tin(IV) Polyazides. *Chem. Eur. J.*, **2015**, *51*, 18690-18698.
(18) Lyhs, B.; Bläser, D.; Wölper, C.; Schulz, S.; Haack, R.; Jansen, G. Synthesis and Structure of Base-Stabilized Germanium(II) Diazide $IPrGe(N_3)_2$. *Inorg. Chem.*, **2013**, *52*, 7236−7241.
(19) Ayers, A. E.; Marynick, D. S.; Dias, H. V. R. Azido Derivatives of Low-Valent Group 14 Elements: Synthesis, Characterization, and Electronic Structure of $[(n\text{-}Pr)_2ATI]GeN_3$ and $[(n\text{-}Pr)_2ATI]SnN_3$ Featuring Heterobicyclic 10-π-electron Ring Systems *Inorg. Chem.*, **2000**, *39*, 4147-4151.
(20) Dias, H. V. R.; Ayers, A. E. Reactions of divalent group 14 compounds containing an azide functionality: synthesis and characterization of $[HB(3,5\text{-}(CF_3)_2Pz)_3]AgGe(N_3)[(n\text{-}Pr)_2ATI]$ and $[HB(3,5\text{-}(CF_3)_2Pz)_3]AgSn(N_3)[(n\text{-}Pr)_2ATI]$. *Polyhedron*, **2002**, *21*, 611-618.
(21) Ayers, A. E.; Klapötke, T. M.; Dias, H. V. R. Azido Derivatives of Germanium(II) and Tin(II): Syntheses and Characterization of $[(Mes)_2DAP]GeN_3$, $[(Mes)_2DAP]SnN_3$, and the Corresponding Chloro Analogues Featuring Heterocyclic Six-π-Electron Ring Systems (where $[(Mes)_2DAP]$) $\{N(Mes)C(Me)\}_2CH$). *Inorg. Chem.*, **2001**, *40*, 1000-1005.
(22) Akkari, A.; Byrne, J. J.; Saur, I.; Rima, G.; Gornitzka, H.; Barrau, J. Three coordinate divalent Group 14 element compounds with a β-diketiminate as supporting ligand L_2MX [L_2 = PhNC(Me) CHC(Me)NPh, X = Cl, I; M = Ge, Sn]. *J. Organomet. Chem.*, **2001**, *622*, 190-198.
(23) Ding, Y.; Roesky, H. W.; Noltemeyer, M.; Power, P. P. Synthesis and Structures of Monomeric Divalent Germanium and Tin Compounds Containing a Bulky Diketiminato Ligand *Organometallics*, **2001**, *20*, 1190-1194.
(24) Leung, W. P.; Kan, K. W.; Chan, Y. C.; Mak, T. C. W. Reactivity Study of a Chlorostannylene Derived from Bis(iminophosphoranyl)-methane *Eur. J. Inorg. Chem.*, **2014** 3191-3199.
(25) Peerless, B.; Keane, T.; Meijer, A. J. H. M.; Portius, P. Homoleptic low-valent polyazides of group 14 elements *Chem. Commun.*, **2015**, *51*, 7435-7438.
(26) Ochiai, T.; Franz, D.; Irran, E.; Inoue, S. Formation of an Imino-Stabilized Cyclic Tin(II) Cation from an Amino(imino)stannylene. *Chem. Eur. J.*, **2015**, *21*, 6704 -6707.
(27) Khrustalev, V. N.; Portnyagin, I. A.; Zemlyansky, N. N.; Borisova, I. V.; Ustynyuk, Y. A.; Antipin, M. Y. New stable germylenes, stannylenes, and related compounds. 5. Germanium(II) and tin(II) azides $[N_3\text{-}E14\text{-}OCH_2CH_2NMe_2]_2$ (E14 = Ge, Sn): synthesis and structure. *J. Organomet. Chem.*, **2005**, *690*, 1056-1062.
(28) Müller, T. G.; Karau, F.; Schnick, W.; Kraus, F. A New Route to Metal Azides. *Angew. Chem. Int. Ed.*, **2014**, *53*, 13695-13697.
(29) Gray, P.; Waddington, T. C. Sensitivity of Alpha- and Beta- Lead Azide. *Nature*, **1955**, *176*, 653.
(30) Fischer, D.; Klapötke, T. M.; Stierstorfer, J. Potassium 1,1'-Dinitramino-5,5'-bistetrazolate: A Primary Explosive with Fast Detonation and High Initiation Power. *Angew. Chem. Int. Ed.*, **2014**, *53*, 8172-8175.
(31) Haiges, R.; Boatz, J. A.; Vij, A.; Gerken, M.; Schneider, S.; Schroer, T.; Christe, K. O. Polyazide chemistry: preparation and characterization of $Te(N_3)_4$ and $[P(C_6H_5)_4]_2[Te(N_3)_6]$ and evidence for $[N(CH_3)_4][Te(N_3)_5]$. *Angew. Chem., Int. Ed.*, **2003**, *42*, 5847-5851.
(32) Haiges, R.; Boatz, J. A.; Schneider, S.; Schroer, T.; Yousufuddin, M.; Christe, K. O. The Binary Group 4 Azides $[Ti(N_3)_4]$, $[P(C_6H_5)_4][Ti(N_3)_5]$, and $[P(C_6H_5)_4]_2[Ti(N_3)_6]$ and on Linear TiNNN Coordination. *Angew. Chem. Int. Ed.*, **2004**, *43*, 3148 -3152.

(33) Haiges, R.; Schroer, T.; Yousuffudin, M.; Christe, K. O. The Syntheses and Structures of Ph_4EN_3 (E = P, As, Sb), an Example for the Transition from Ionic to Covalent Azides within the Same Main Group. *Z. Anorg. Allg. Chem.*, **2005**, *631*, 2691-2695.
(34) Haiges, R.; Rahm, M.; Christe, K. O. Unprecedented conformational variability in main group inorganic chemistry: the tetraazidoarsenite and -antimonite salts $A^+ [M(N_3)_4]^-$ (A = NMe_4, PPh_4, $(Ph_3P)_2N$; M = As, Sb), five similar salts, five different anion structures. *Inorg. Chem.*, **2013**, *52*, 402-414.
(35) Deokar, P.; Vasiliu, M.; Dixon, D. A.; Christe, K. O.; Haiges, R. The Binary Group 4 Azides $[PPh_4]_2[Zr(N_3)_6]$ and $[PPh_4]_2[Hf(N_3)_6]$. *Angew. Chem., Int. Ed.*, **2016**, *55*, 14350-14354.
(36) Villinger, A.; Schulz, A. Binary Bismuth(III) Azides: $Bi(N_3)_3$, $[Bi(N_3)_4]^-$, and $[Bi(N_3)_6]^{3-}$. *Angew. Chem. Int. Ed.*, **2010**, *49*, 8017–8020.
(37) Haiges, R.; Boatz, J. A.; Williams, J. M.; Christe, K. O. Preparation and Characterization of the Binary Group 13 Azides $M(N_3)_3$ and $M(N_3)_3{\cdot}CH_3CN$ (M = Ga, In, Tl), $[Ga(N_3)_5]^{2-}$, and $[M(N_3)_6]_3$ (M = In, Tl). *Angew. Chem. Int. Ed.*, **2011**, *50*, 8828-8833.
(38) Klapötke, T. M.; Krumm, B.; Scherr, M.; Haiges, R.; Christe, K. O. The binary selenium(IV) azides $Se(N_3)_4$, $[Se(N_3)_5]^-$, and $[Se(N_3)_6]^{2-}$ *Angew. Chem., Int. Ed.*, **2007**, *46*, 8686-8690.
(39) Avrami, L.; Hutchinson, R. Sensitivity to Impact and Friction. *Energetic Materials, H. D. Fair, R. F. Walker (ed.)*, **1977**, *Vol. 2*, 111-159.
(40) Fenske, D.; Dörner, H. D.; Dehnicke, K. The crystal structure of bis(tetraphenylphosphonium) hexaazidostannate $[(Ph_4P)_2[Sn(N_3)_6]]$. *Z. Naturforsch. B Chem. Sci.*, **1983**, *38B*, 1301-1303.
(41) Dias, H. V. R.; Ayers, A. E. Reactions of divalent group 14 compounds containing an azide functionality: synthesis and characterization of $[HB(3,5\text{-}(CF_3)_2Pz)_3]AgGe(N_3)[(n\text{-}Pr)_2ATI]$ and $[HB(3,5\text{-}(CF_3)_2Pz)_3]AgSn(N_3)[(n\text{-}Pr)_2ATI]$. *Polyhedron*, **2002**, *21*, 611-618.
(42) Pacher, A.; Schrenk, C.; Schnepf, A. Sn(II) halides: Novel binary compounds of tin and their application in synthetic chemistry. *J. Organomet. Chem.*, **2010**, *695*, 941-944.
(43) Bondi, A. van der Waals Volumes and Radii. *J. Phys. Chem.*, **1964**, *68*, 441-451.
(44) Alvarez, S. A Cartography of the van der Waals Territories. *Dalton Trans.*, **2013**, *42*, 8617-8636.
(45) Desiraju, G. R.; Steiner, T. *The Weak Hydrogen Bond in Structural Chemistry and Biology*, **1999**, *Oxford University Press, Oxford*, p12ff.
(46) Szafrański, M. Effect of High Pressure on the Supramolecular Structures of Guanidinium Based Ferroelectrics. *CrystEngComm*, **2014**, *16*, 6250-6256.
(47) Petříček, V.; Dušek, M.; Palatinus, L. Crystallographic Computing System JANA2006: General features. *Z. Kristallogr.*, **2014**, *229*, 345-352.
(48) Mcdonald, R. C.; Hau, H. H. K.; Eriks, K. Crystallographic Studies of Tin(II) Compounds. I. Crystal Structure of Tin(II) Fluoride, SnF_2. *Inorg. Chem.*, **1976**, *15*, 762-765.
(49) Jones, D. A. Growth of Lead Fluoride from the Melt. *Proc. Phys. Soc. B*, **1955**, *68*, 165-170.
(50) Berg, J. M. V. D. The Crystal Structure of $SnCl_2$. *Acta Cryst.*, **1961**, *14*, 1002-1003.
(51) Sass, R. L.; Brackett, E. B.; Brackett, T. E. Crystal Structure of Lead Chloride. *J. Phys. Chem.*, **1963**, *67*, 2863-2964.
(52) Birkofer, L.; Ritter, A.; Richter, P. Silicon-Organic Compounds. XIV. Preparation of Trimethylsilyl Azide. *Angew. Chem.*, **1962**, *74*, 293.
(53) Birkofer, L.; Wegner, P. Trimethylsilyl azide. *Org. Synth.*, **1970**, *50*, 107-110.
(54) Fulmer, G. R.; Miller, A. J. M.; Sherden, N. H.; Gottlieb, H. E.; Nudelman, A.; Stoltz, B. M.; Bercaw, J. E.; Goldberg, K. I. NMR Chemical Shifts of Trace Impurities: Common Laboratory Solvents, Organics, and Gases in Deuterated Solvents Relevant to the Organometallic Chemist. *Organometallics*, **2010**, *29*, 2176-2179.
(55) Sheldrick, G. M. A Short History of SHELX. *Acta Cryst. A*, **2008**, *64*, 112-122.
(56) Farrugia, L. J. WinGX and ORTEP for Windows: an update *J. Appl. Crystallogr.*, **2012**, *45*, 849-854.
(57) Farrugia, L. J. WinGX Suite for Small-Molecule Single-Crystal Crystallography. *J. Appl. Crystallogr.*, **1999**, *32*, 837-838.
(58) Pawley, G. S. Unit-Cell Refinement from Powder Diffraction Scans. *J. Appl. Crystallogr.*, **1981**, *14*, 357-361.
(59) Clark, S. J.; Segall, M. D.; Pickard, C. J.; Hasnip, P. J.; Probert, M. J.; Refson, K.; Payne, M. C. First Principles Methods Using CASTEP *Z. Kristallogr.*, **2005**, *220*, 567-570.

(60) Tkatchenko, A.; Scheffler, M. Accurate Molecular Van Der Waals Interactions from Ground-State Electron Density and Free-Atom Reference Data. *Phys. Rev. Lett.*, **2009**, *102*, 073005/073001-073005/073004.
(61) Perdew, J. P.; Burke, K.; Ernzerhof, M. Generalized Gradient Approximation Made Simple. *Phys. Rev. Lett.*, **1996**, *77*, 3865-3868.
(62) Vackar, J.; Hytha, M.; Simunek, A. All-Eelectron Pseudopotentials. *Phys. Rev. B*, **1998**, *58*, 12712-12720.
(63) Monkhorst, H. J.; Pack, J. D. Special Points for Brillonin-Zone Integrations. *Phys. Rev. B*, **1976**, *13*, 5188-5192.
(64) Fischer, T. H.; Almlof, J. General Methods for Geometry and Wave Function Optimization. *J. Phys. Chem.*, **1992**, *96*, 9768-9774.